



CrossMark
click for updates

Cite this: *Nanoscale*, 2016, **8**, 3555

Ultra-large suspended graphene as a highly elastic membrane for capacitive pressure sensors†

Yu-Min Chen,^{a,b} Shih-Ming He,^a Chi-Hsien Huang,^c Cheng-Chun Huang,^d Wen-Pin Shih,^d Chun-Lin Chu,^e Jing Kong,^f Ju Li^g and Ching-Yuan Su^{*a,b,h}

In this work, we fabricate ultra-large suspended graphene membranes, where stacks of a few layers of graphene could be suspended over a circular hole with a diameter of up to 1.5 mm, with a diameter to thickness aspect ratio of 3×10^5 , which is the record for free-standing graphene membranes. The process is based on large crystalline graphene ($\sim 55 \mu\text{m}$) obtained using a chemical vapor deposition (CVD) method, followed by a gradual solvent replacement technique. Combining a hydrogen bubbling transfer approach with thermal annealing to reduce polymer residue results in an extremely clean surface, where the ultra-large suspended graphene retains the intrinsic features of graphene, including phonon response and an enhanced carrier mobility (200% higher than that of graphene on a substrate). The highly elastic mechanical properties of the graphene membrane are demonstrated, and the *Q*-factor under 2 MHz stimulation is measured to be 200–300. A graphene-based capacitive pressure sensor is fabricated, where it shows a linear response and a high sensitivity of 15.15 aF Pa^{-1} , which is 770% higher than that of frequently used silicon-based membranes. The reported approach is universal, which could be employed to fabricate other suspended 2D materials with macro-scale sizes on versatile support substrates, such as arrays of Si nano-pillars and deep trenches.

Received 6th December 2015,

Accepted 11th January 2016

DOI: 10.1039/c5nr08668j

www.rsc.org/nanoscale

Introduction

Freestanding 2D membranes provide new functions to materials and devices. For example, reported works demonstrate suspended highly ordered and elastic membranes formed by the self-assembly of nanomaterials such as nanoparticles or nanowires, which show potential for use in nano-

devices and sensor applications.^{1–5} Graphene, an atomic layer of graphite, has attracted intense interest in the last few decades.⁶ The earlier studies on graphene were usually performed on supporting substrates such as SiO_2/Si . However, substrate induced carrier scattering, dopants and phonon leakage significantly obscured the intrinsic properties of graphene. Recent studies on suspended graphene have revealed superior physical and chemical properties, and have provided ultimate platforms for exploiting the properties of pristine graphene, such as the extremely high carrier mobility ($\sim 200\,000 \text{ cm}^2 \text{ V}^{-1} \text{ s}^{-1}$),⁷ high mechanical strength ($\sim 130 \text{ GPa}$),⁸ and superior thermal conductivity ($\sim 5300 \text{ W mK}^{-1}$).⁹ All of these unique properties have spurred various fundamental research topics, including atomic layer mechanics,^{10–12} electronic transport, and heat propagation.¹³ Additionally, suspended graphene has been proposed for many exciting applications in future technologies, such as electromechanical resonators/actuators,¹⁴ higher performance biological membranes, sensors for DNA sequences and cancer detection,^{15,16} piezoresistive pressure sensors,¹⁷ bright visible light emissions,¹⁸ high responsivity photodetectors,¹⁹ gas impermeable membranes or permeance membranes for gas, liquid or molecular separation,^{20,21} and high resolution TEM imaging on wet biological samples.^{22–25} Most of these potential applications require large-area, extremely thin ($<10 \text{ nm}$), and residue-free membranes, therefore suspended graphene is an ideal candi-

^aGraduate Institute of Energy Engineering, National Central University, Tao-Yuan 32001, Taiwan. E-mail: cysu@ncu.edu.tw

^bDep. of Mechanical Engineering, National Central University, Tao-Yuan 32001, Taiwan

^cDep. of Materials Engineering, Ming Chi University of Technology, New Taipei City 24301, Taiwan

^dDep. of Mechanical Engineering, National Taiwan University, Taipei City 10617, Taiwan

^eNational Nano Device Laboratories, Hsinchu, 30078, Taiwan

^fDepartment of Electrical Engineering and Computer Sciences, Massachusetts Institute of Technology, 77 Massachusetts Avenue, Cambridge, MA 02139, USA

^gDepartment of Nuclear Science and Engineering and Department of Materials Science and Engineering, Massachusetts Institute of Technology, Cambridge, Massachusetts 02139, USA

^hGraduate Institute of Material Science and Engineering, National Central University, Tao-Yuan 32001, Taiwan

†Electronic supplementary information (ESI) available: The detailed process/recipe for CVD-grown graphene and the transferring process, SEM and TEM images, contact angles, force curves, and movie clips. See DOI: 10.1039/c5nr08668j

date in this regard. However, there is still no reliable approach to prepare suspended graphene on a macro-scale size, *i.e.*, larger than a millimeter scale, mainly due to the rupture force on the graphene membrane from the surface tension of the liquid during wet-etching and drying procedures. The obtained size based on the conventional approach is limited to a few micrometers in diameter.^{26,27} In recent works on obtaining free-standing graphene membranes, graphene was first transferred to a substrate, followed by critical point drying to avoid the drag force from surface tension.^{12,28} With this approach, the size could be improved to a few tens of micrometers. However, this size is still limited for most applications, and an additional issue is the introduction of unwanted impurities and residues on the graphene surface by employing this drying method. In 2014, Lee *et al.*, published a strategy called an inverted floating method in which acetone is gradually replaced by a solvent with a low surface tension to lower the drag force when drying, resulting in a suspended graphene membrane up to ~ 500 μm in diameter.²⁹ However, it was found to suffer from a large amount of polymer residue on the graphene surface. This residue issue is crucial for specific applications, such as chemical/bio-medical sensors, that require an extremely clean graphene surface for ultra-sensitive sensing. Therefore, the development of large scale, free-standing, and clean graphene membranes for the aforementioned applications is of great importance.

Suspended graphene membranes have been demonstrated to be promising materials for electromechanical piezoresistive pressure sensors, which show sensitivity orders of magnitude greater than other membrane materials, such as silicon and carbon nanotubes (CNTs).¹⁷ Recently, capacitive pressure sensors have been intensively investigated because of their widespread applications in medicine, aerospace, and automobiles due to the advantages of high sensitivity, low temperature dependence, higher signal response and lower power consumption when compared to piezoresistive-type sensors. In general, a high sensitivity capacitive pressure sensor requires (1) a larger membrane area, (2) a reduced membrane thickness, and (3) a decreased sensing gap.³⁰ Therefore, a suspended graphene membrane is an ideal candidate in this regard.

In this work, we demonstrate a novel method to yield the largest (up to 1.5 mm) and highest quality suspended graphene membranes through solvent replacement, followed by thermal decomposition. X-ray photoelectron spectroscopy (XPS) characterization shows an extremely clean graphene membrane with a low amount of oxygen functional groups (4–6%). To demonstrate a potential application based on this ultra-large suspended graphene, a pressure sensor was created. The as-prepared graphene-based capacitive pressure sensor shows a sensitivity of 15.15 aF Pa^{-1} , which is 770% higher than that of conventional silicon-based materials made with micro-fabrication technologies. This study sheds light on the development of atomic layered devices and addresses the present bottleneck in bridging applications from the nano- to the macro-scale, while preserving the high performance

intrinsic properties of graphene. Additionally, ultra-large free-standing graphene or other 2D layered membranes could be applied as an ideal platform to exploit new chemical/physical phenomena down to the atomic scale.

Results and discussion

The graphene film used in this work was synthesized using an atmospheric pressure CVD (APCVD) method (see the Experimental section for details). To obtain high mechanical strength graphene films for the subsequent fabrication of suspended membranes, graphene sheets with large single crystalline domains were obtained by comprehensively studying and optimizing the growth process conditions (see S1†). Fig. 1a shows the SEM image of a graphene domain, where the white-line denotes the defined lateral size of a single crystalline domain. Fig. 1b shows the statistical analysis of the graphene domain size according to various growth conditions. The results clearly reveal that the three conditions of 1045 $^{\circ}\text{C}$ with $\text{H}_2 = 20$ sccm, and 1060 $^{\circ}\text{C}$ with $\text{H}_2 = 20$ and 30 sccm yielded relatively large domain sizes. Subsequently, continuous graphene films were obtained by extending the growth time based on these three conditions. The as-grown samples were further characterized using Raman spectroscopy and Hall measurements to verify the quality. Fig. 1c shows the Raman spectra for these three samples, where the case of 1060 $^{\circ}\text{C}/\text{H}_2 = 20$ shows a lower D/G intensity ratio, indicating a low defect density. Further characterization of the AFM height profile (~ 0.78 nm in Fig. 1d) and cross-section TEM image for the sample (Fig. S2†) shows a uniform single-layered graphene film. In addition, the sheet resistance and optical transparency were characterized (see Fig. S1–3†), exhibiting the lowest sheet resistance of 592 ohm sq^{-1} at an optical transmittance of $\sim 97\%$, suggesting single layered graphene and a lower density of the graphene boundary in the obtained film. Thus, the following suspended graphene membranes in this study were synthesized under these conditions.

The detailed procedure for fabricating the suspended graphene samples can be found in the Experimental section. Briefly, five-layer (5L) graphene was made using layer-by-layer stacking, and then it was transferred onto substrates with holes using supporting polymethyl methacrylate (PMMA) layers, where the hole diameters ranged from a few tens of micrometers to two millimeters (Fig. 2a). It is clearly observed that the graphene/PMMA composite film remained well-suspended over the holes without rupturing, mainly due to the high strength of the supporting PMMA layers (Fig. 2b).

Unlike previous work where the PMMA layer was removed with acetone causing the graphene film to easily rupture when the solution dried, a solvent replacement approach was employed in this study. Fig. 2c illustrates the experimental setup, where the sample is placed face down and bridges a channel. Acetone was gradually streamed into the channel, and the PMMA layer was then removed when the flow contacted the surface. After 10 min, the solution was switched

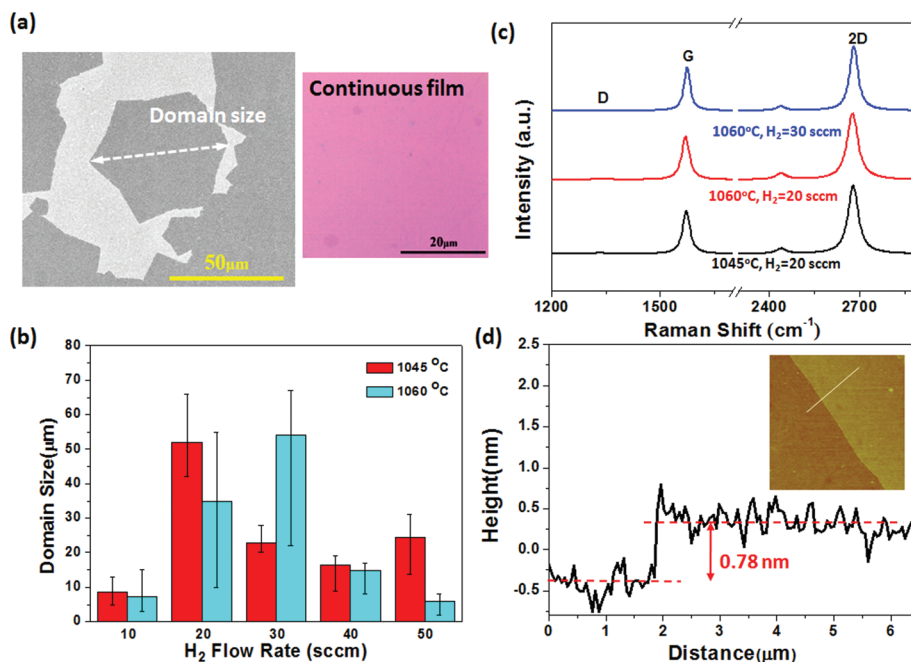


Fig. 1 (a) Typical SEM image of a single-crystalline graphene domain grown using APCVD. The right image is an optical image for the continuous graphene film that was transferred onto a SiO₂/Si substrate. (b) Statistical analysis on the graphene domain sizes for various growth conditions, showing that a relatively larger domain size could be obtained under the following conditions: 1045 °C (H₂ = 20 sccm), 1060 °C (H₂ = 20 sccm) and 1060 °C (H₂ = 30 sccm). (c) Typical Raman spectra for these three samples. (d) AFM height profile for the samples prepared under the conditions of 1060 °C (H₂ = 30 sccm), indicating a uniform thickness of 0.78 nm.

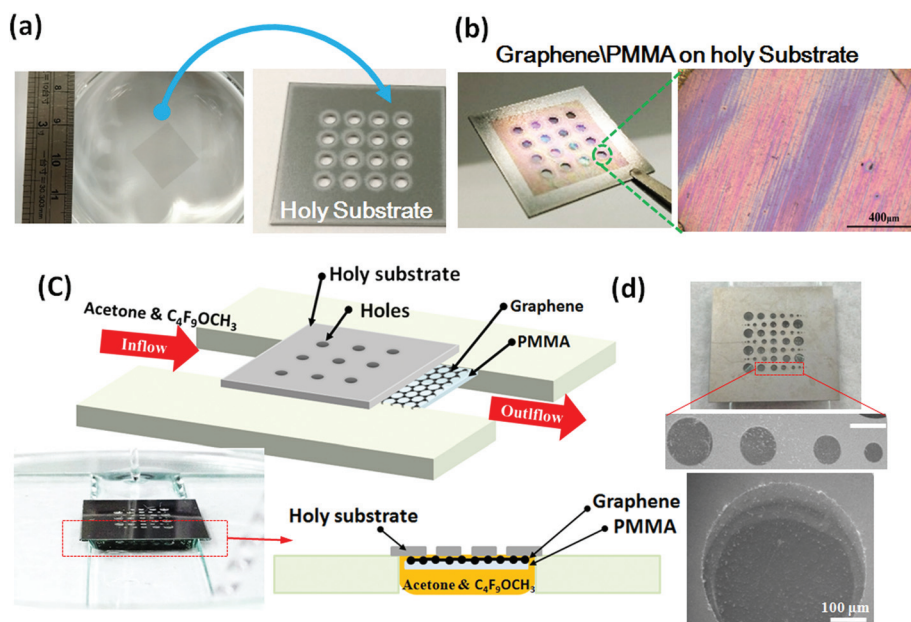


Fig. 2 The transferring procedure for fabricating ultra-large suspended graphene membranes. (a) The optical images of a graphene/PMMA composite film floating on the surface of water and receiving a stainless steel substrate with holes. (b) The PMMA/graphene composite film was transferred onto the substrate with holes without rupturing. (c) Schematic illustration of the procedures involved in the solvent replacement method, where a pristine graphene membrane could be well-suspended across the substrate with holes without rupturing when PMMA was removed and dried with a low surface tension solvent. (d) Optical and SEM images of graphene successfully suspended over circular holes 600 μm–1200 μm in diameter. The scale bar is 1 mm.

from acetone to a low surface tension solvent, *i.e.*, methoxy-nonafluorobutane ($C_4F_9OH_3$). It was found that the 5L graphene membrane could be suspended over the substrate with holes of diameters ranging from 200 μm up to 1.5 mm, as shown in Fig. 2d. To prevent the rupture of the membrane, the drag force, induced during the solvent drying process, needs to be considered and it depends on a combination of quite a few factors, such as density, viscosity, velocity *etc.*, and among them, the surface tension is regarded as the dominant factor. Therefore, it is of great importance to further examine the surface tension. Fig. S3[†] shows the contact angle measurements, where the contact angles are water (89.58°), acetone (13.52°), and $C_4F_9OH_3$ (10.57°), indicating that a lower surface tension can significantly lower the drag force and does not lead to the rupture of the suspended graphene membrane when drying.

Note that the suspended membrane of single layer graphene was limited to an approximately 600 μm hole diameter by the same process. In the case of the 1.5 mm hole, it was found out that the stacking layers with 1–4 layers were unable to obtain a full-coverage film without rupturing, indicating that the stacking of up to five layers of graphene can provide sufficient mechanical strength to compensate for the rupture force arising from the surface tension of the solvent. Fig. 3a and b show the Raman spectra for single-layered suspended graphene and substrate-supported single-layered graphene, where a narrow band width of 33 cm^{-1} and the down shifting

of G and 2D bands were clearly observed for the suspended graphene sample. This result indicates that graphene is free from interaction from the substrate, and this feature is consistent with the reported work on suspended graphene films.³¹

By employing the solvent replacement method for 5-layered graphene, it was found that the largest suspended graphene membranes over 1.5 mm diameter holes can be successfully obtained as shown in Fig. 3c (the yield rate is $\sim 10\%$). To the best of our knowledge (see Table S7[†] for this comparison), this was the largest suspended graphene membrane. In addition to the solvent replacement method, a direct thermal decomposition approach was carried out for preparing suspended graphene membranes, where the samples were subject to thermal annealing under a fuming gas atmosphere (H_2/Ar) to remove the PMMA supporting layers (see the Experimental section). In this case, the yield rate (for a 1.5 mm diameter hole) was doubled compared to that for the solvent replacement method, indicating that direct sublimation to decompose PMMA polymer could be a more reliable method for yielding large-area suspended graphene. Fig. 3d shows the statistical analysis of the yield rate for these two methods, indicating the significantly increased yield rate for the thermal decomposition approach, especially for large holes with diameters ranging from 600 to 1500 μm .

However, by employing the thermal decomposition method, it was found that an unwanted non-crystalline phase of carbon appeared on the as-prepared graphene surface.

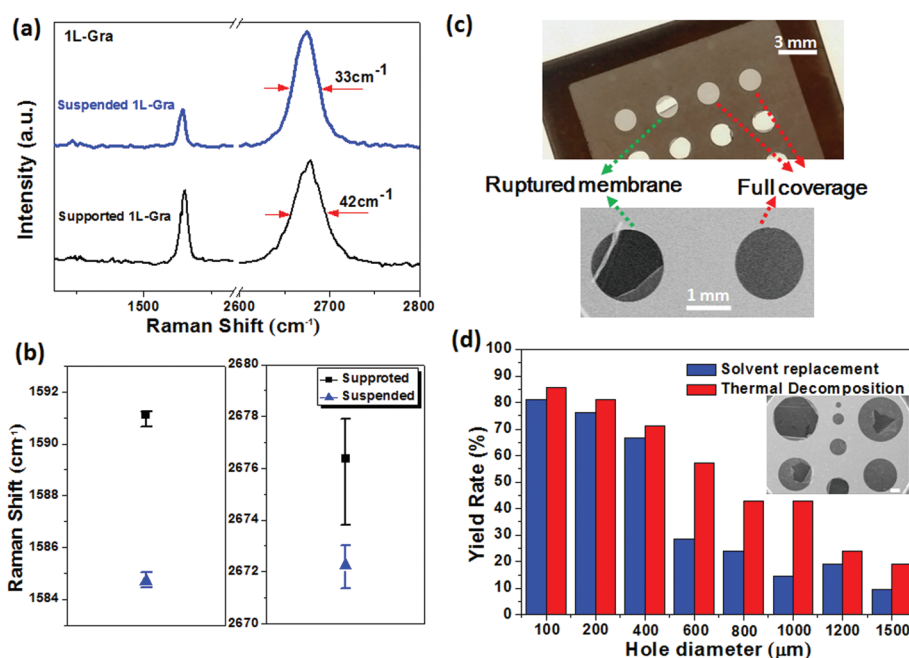


Fig. 3 (a) Comparison of the typical Raman feature peaks (G and 2D) for the cases of substrate-supported single-layered (1L-) graphene and the suspended 1L-graphene membrane. (b) The corresponding peaks positions of G and 2D peaks for the substrate-supported and suspended graphene samples. (c) The optical and SEM images for the ruptured and full coverage graphene membranes on the substrate with 1.5 mm diameter holes. (d) Histogram of the statistical yield rate for the various hole diameters using the solvent replacement and thermal decomposition method. The inset shows the SEM image of test samples (the scale bar is 300 μm), where the yield is defined as the full coverage of the membrane without any cracks or ruptures.

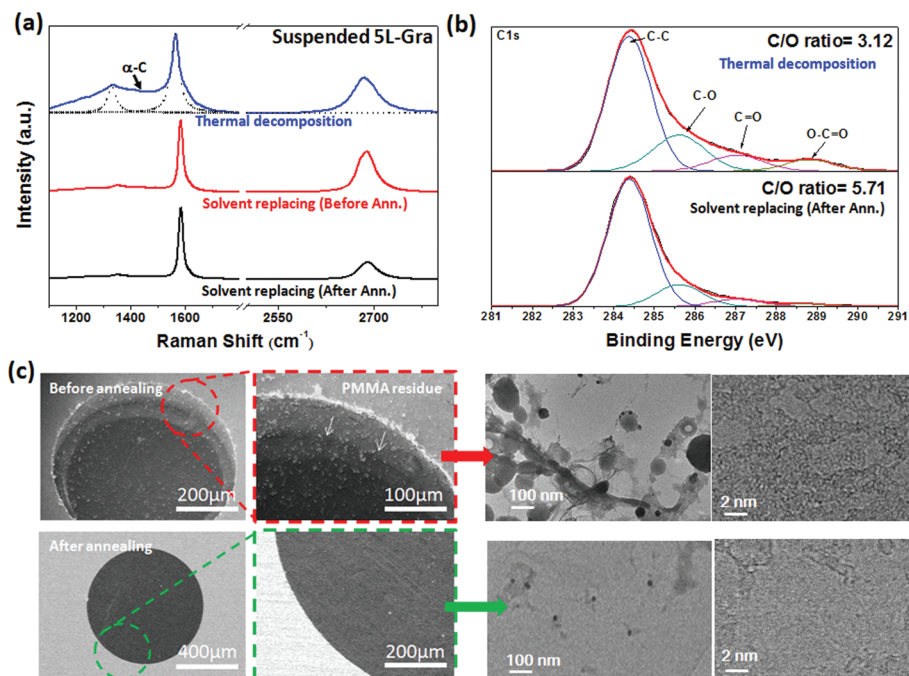


Fig. 4 (a) Raman spectra for the suspended 5L graphene membranes made using three approaches, *i.e.*, thermal decomposition and solvent replacement methods with/without post-annealing. (b) Comparison of the XPS C 1s spectra for the graphene membranes made through solvent replacement with/without post-annealing. (c) Comparison of the surface morphologies and nanostructures using SEM and HRTEM images for samples with/without post-annealing, indicating the efficient removal of PMMA residue (denoted by white arrows) when subjected to post-annealing.

Fig. 4a shows the typical Raman spectra for suspended graphene made using the three different approaches. The pronounced broad peak between the G and D bands was clearly seen for the sample made with direct thermal annealing, which was due to the non-crystalline carbon phase as denoted by amorphous carbon (α -C) in the spectrum. This was attributed to the carbonization of polymer from the thick PMMA layer during the thermal decomposition process, where the PMMA directly transforms to α -C and remains on the graphene surface rather than a gradual sublimation.

Moreover, the XPS characterization shows that 36.6% of the oxidized functional groups (mainly C-O, C=O and O-C=O) were on the surface (Fig. 4b). The existence of a large amount of unwanted α -C and oxidized functional groups over the graphene surface led to the degradation of the intrinsic graphene properties (see Fig. S4† for detailed nanostructure characterization). In addition to samples from the thermal decomposition method, the Raman spectrum was taken for the sample prepared using the solvent replacement method (red spectrum in Fig. 4a), where the α -C signal was not observed, and the crystallinity increased when it was further annealed to remove residual PMMA (black spectrum in Fig. 4a). Fig. 4c shows the SEM and TEM images for the suspended graphene prepared using the solvent replacement method. The results indicate a large amount of polymer residue on the graphene surface when it was treated only with acetone and solvent, while the additional thermal treatment significantly reduced the amount of polymer to obtain a cleaner graphene sample. The

XPS analysis in Fig. 4b shows a highly improved C/O ratio of 5.17, suggesting a lower amount of carbon-oxygen species on the surface. The aforementioned results clearly demonstrate that the suspended graphene quality, with respect to the crystallinity and cleanliness of the surface, was optimized using the solvent replacement method and subsequent thermal annealing.

Moreover, it is well-known that in the conventional graphene transferring process, by employing an etching solution (such as FeCl₃) to remove the Cu substrate, residual metal iron/clusters are found to aggregate and distribute over the graphene surface. Fig. 5a shows the optical image of 5L suspended graphene made using the FeCl₃ etching process followed by careful dilution with hydrochloride and DI-water several times, which reveals a large amount of impurity on the surface. Further XPS characterization to obtain the Cu 2p spectra indicates the existence of Cu metal residues on the graphene surface (Fig. 5c). Employing a hydrogen bubbling transfer technique, as reported in previous work,³² can remarkably yield extremely clean and metal-free graphene as shown in Fig. 5b and c. The surface is uniform (approximately 5 nm in thickness over the membrane) and clean as shown by the AFM image in Fig. 5d, suggesting that the bubbling transfer method provides a higher quality of suspended graphene membranes.

The aforementioned technique provides a reliable route to produce large-area suspended membranes down to a few atomic layers. This technology is not limited to substrates with

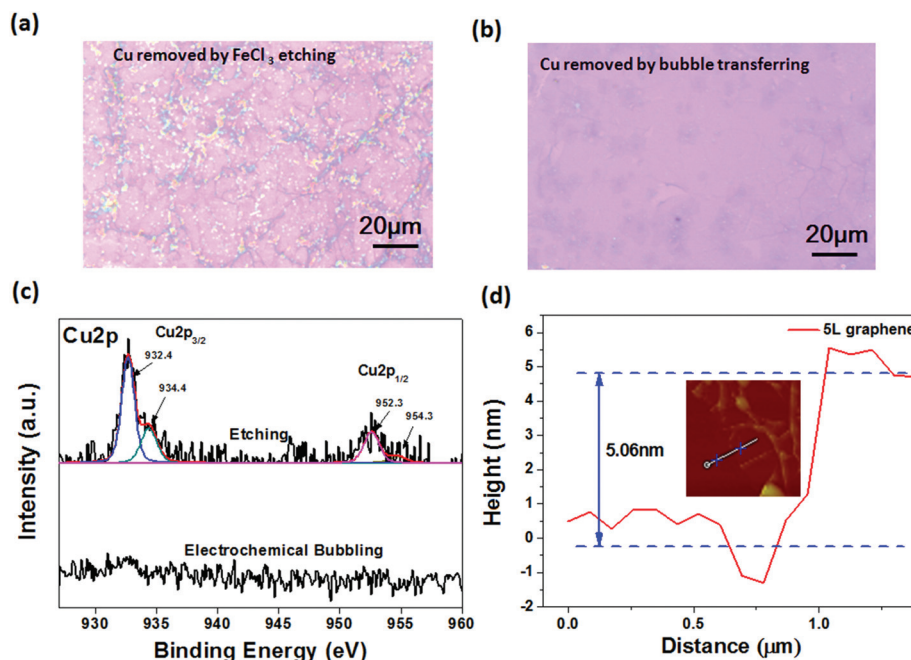


Fig. 5 Typical optical images for the 5L graphene samples prepared using (a) conventional Cu etching and (b) the bubbling transfer method. (c) The corresponding XPS Cu2p spectra for these two graphene membranes. (d) AFM image and height profile for the samples prepared using the bubbling transfer method.

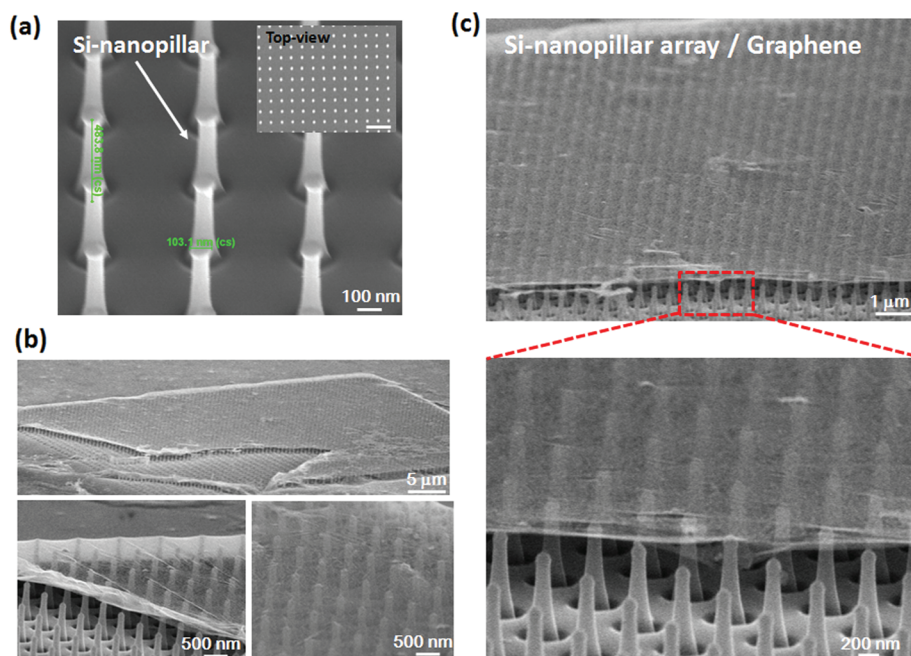


Fig. 6 A single-layered graphene membrane suspended on a prefabricated substrate of an ordered array of Si nano-pillars. (a) SEM image of the fabricated Si nano-pillars. The inset shows a top-view image of the substrate (scale bar: 1 μm). (b) Image of suspended graphene over a macro-size array of 25 μm . (c) Magnified image of nano-pillar supported graphene, showing a uniform and wrinkle-free surface.

holes and can be extended to substrates with more complex structures. Fig. 6 shows the SEM images for single-layered graphene suspended on a prefabricated substrate of an ordered array of Si nano-pillars, where the nano-pillars have a height of

480 nm and a diameter of 103 nm, arranged with a pitch of 500 nm (Fig. 6a). Fig. 6b and c show that graphene can lie fully suspended over a length scale of 25 μm with minimal point contacts with the apexes of the Si nano-pillars without col-

lapse. Graphene supported onto the periodic array of pillars offers a unique platform to alter the stress in graphene layers where the strain domains are periodically arranged. The so-called strain superlattice in graphene was first reported in 2014 by designing specific geometries of pitch and density of nano-pillar arrays,³¹ which was regarded as a promising strategy for engineering the electrical bandgap and optical conductivity of graphene due to the ripple-free features in graphene. However, graphene collapse occurs during the conventional transferring process, which obstructs the versatile design of the strain superlattice. Our proposed technique in this study can address this issue by fabricating a larger size of suspended graphene bridging over a large pitch between the pillars without collapsing. This leads to the potential applications of the strain superlattice, such as in high mobility nanoelectronics and photonic devices. Moreover, this unique structure might create a new platform to study new physical properties, such as electron/phonon transport on graphene, since the interaction from the substrate becomes minimal when the suspended graphene is altered by a point-like contact with periodic substrate interactions.

To examine the potential applications of the as-prepared ultra-large suspended graphene membranes, a capacitive pressure sensor based on the graphene membrane was first demonstrated in this investigation. Fig. 7a illustrates the proof-of-concept for this device, where the graphene membrane was suspended across a quartz substrate with a circular hole (1.5 mm in diameter) and sealed in a small chamber. When gas flows into the chamber, the induced deformation of

the graphene membrane changes the capacitance between the fixed electrode and the graphene diaphragm. The real-time capacitance and chamber pressure were recorded using a LCR meter and pressure gauge. Fig. 7b shows the optical images for the ballooned graphene membrane, and the largest deformation is approximately 100 μm (see Movie Clip 01† for the dynamic deformation of the membrane). In general, the performance of a capacitive pressure sensor is expressed according to the constructed model as shown below:

$$\frac{\Delta C}{P} = \frac{3(1-\nu^2)R^4 \epsilon_0 \epsilon_r A_{\text{sense}}}{16ET^3 g^2}$$

where ΔC = the change in capacitance, P = the pressure difference, R = radius of the diaphragm, T = thickness of the diaphragm, E = Young's modulus of the diaphragm material, ν = Poisson's ratio of the diaphragm material, ϵ_0 = permittivity, ϵ_r = relative static permittivity, A_{sense} = the area of the moving plate and g = the sensing gap between the moving plate and the fixed plate. Therefore, in principle, the increased ratio of R/T results in higher sensitivity.³⁰ The capacitance of the sensor is a function of the separation between the fixed electrode and the graphene membrane. When the graphene deforms close to the electrode, the capacitance increases and *vice versa*. The performance characterization of the capacitive pressure sensor is shown in Fig. 7c, where the sensitivity was defined as the capacitance change per unit pressure difference ($\Delta C/\Delta P$). The curve revealed the linear characteristic of the pressure response. Moreover, 5L graphene shows much better reliability and stability than the 1L graphene film during the

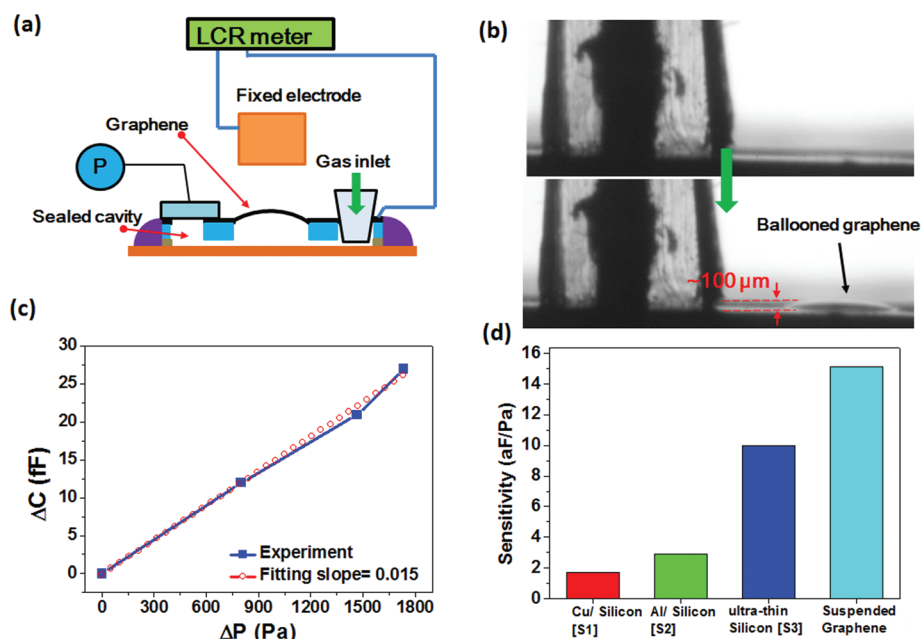


Fig. 7 Application of a graphene-based capacitive pressure sensor. (a) Schematic illustration of the sensor design and setup. A LCR meter was used for real-time recording of the capacitance variation. (b) Optical images of the ballooned graphene membrane when the gas flows into the chamber, where the suspended diameter is 1.5 mm and the estimated deformation is $\sim 100 \mu\text{m}$. (c) The correlation of capacitance change and measured pressure variations; the sensitivity is defined as $\Delta C/\Delta P$. (d) Histogram of the sensitivity for this work compared to other conventional capacitive pressure sensors made using Cu/Si, Al/Si, and ultra-thin Si membranes (denoted S1–S3^{33,34}) with MEMS technologies.

sensing operation. It was found out that 5L graphene could sustain a pressure difference (ΔP) up to 1800 Pa without rupturing. By controlling the limitation of the pressure difference at less than 1900 Pa, the device shows excellent reliability and long term stability at least up to ~ 200 cycles. Fig. 7d compares the sensitivity obtained from this work to other conventional capacitive pressure sensors. The estimated sensitivity for the graphene-based pressure sensor is 15.2 aF Pa^{-1} , which is superior to the Micro-Electro-Mechanical Systems (MEMS) capacitive pressure sensors where the actuated diaphragms are composed of Cu/Si (1.7 aF Pa^{-1}), Al/Si (2.9 aF Pa^{-1}), and ultra-thin Si membranes (10 aF Pa^{-1}), with thickness to diameter ratios of $25 \text{ }\mu\text{m}/1.2 \text{ mm}$, $25 \text{ }\mu\text{m}/572 \text{ }\mu\text{m}$, and $1.5 \text{ }\mu\text{m}/90 \text{ }\mu\text{m}$, respectively.^{33,34} The results clearly indicate that the as-prepared macro-sized suspended graphene membrane exhibits a higher reversible elasticity than any other known thin-film material today because graphene in this example shows an ultra-high aspect ratio of thickness to diameter of up to 3×10^5 . Very recent work has demonstrated a wideband microphone and an ultrasonic radio made using multi-layered (~ 20 layers) suspended graphene as the diaphragm, which is beneficial for advanced communication technology in the future.³⁵ The large area graphene membrane with an ultra-high aspect ratio in this work shows excellent sensitivity and mechanical strength, which makes it a potential candidate for the aforementioned applications in advanced communication.

In addition, the mechanical properties of the graphene membrane are of great interest. Fig. S5† shows the force curve for the suspended graphene membrane recorded using AFM. The resultant graphene still retained its strength and elastic properties without fracturing even at the deformation limit of the AFM tip of $\sim 5.5 \text{ }\mu\text{m}$ (see Movie Clip 02†). Moreover, the highly elastic mechanical properties of the graphene membrane were studied, and the Q -factor under 2 MHz was measured to be 200–300 using a LCR meter. Although here we demonstrate the outstanding performance of the pressure sensor by employing our ultra-large suspended graphene, it is believed that this technique could be readily applied to other versatile applications. For example in Fig. S6,† we demonstrate that the suspended graphene membrane can be bridged over a long ($\sim 0.5 \text{ cm}$) trenched substrate (SiO_2/Si) with a trench width of approximately $300 \text{ }\mu\text{m}$. By employing the Hall measurement, the result shows that the hole carrier concentration for suspended graphene is 37-fold lower than that of the substrate-supported graphene samples, indicating significantly reduced charge doping from the substrate. In addition, the normalized carrier mobility for suspended graphene is 224% ($2060 \text{ cm}^2 \text{ v}^{-1} \text{ s}^{-1}$ on average) higher than that of the substrate-supported graphene samples ($920 \text{ cm}^2 \text{ v}^{-1} \text{ s}^{-1}$ on average). This result showing the high carrier mobility in micro-fluid-trenches demonstrates the potential application in ultra-sensitive bio-sensors. Another example of utilizing suspended graphene is in highly sensitive touch or motion sensors (see Movie Clip 03†), where the graphene membrane exhibits an ultrafast response when subjected to knocking or environmental vibrations.

Conclusion

In conclusion, we proposed a fabrication method to prepare an ultra-large high-quality suspended graphene membrane, where a stack of 5 layers of graphene could be suspended across a circular hole with a diameter of up to 1.5 mm. The aspect ratio was 3×10^5 , which is a record for free-standing graphene membranes. The process is based on the growth of large crystalline graphene *via* CVD ($\sim 55 \text{ }\mu\text{m}$), followed by a gradual solvent replacement technique. The utilization of a bubbling transfer approach and solvent replacement, as well as thermal annealing methods, led to the large areas and extremely clean surfaces of the graphene membranes. A graphene-based capacitance pressure sensor was first demonstrated, showing linear characteristics and a high sensitivity of 15.15 aF Pa^{-1} , which is 770% higher than that of conventional silicon-based membranes. The reported approach is universal on versatile substrates, such as arrays of Si nano-pillars and deep trenches. This work could not only pave a way for exploiting new physics/chemistry of intrinsic 2D layered materials but can also shed light on their potential applications in the future.

Experimental

Synthesis of large single crystal graphene

Prior to the CVD growth process, Cu foil (Alfa Aesar 99.8%; $25 \text{ }\mu\text{m}$) was subjected to a surface flattening process using electrochemical polishing, where the Cu foil was placed in the anode and a Cu plate was employed as the cathode with a separation of 10 cm in an electrolyte mixture of 70 wt% H_3PO_4 (Nihon Shiyaku 85%) with polyethylene glycol (Alfa Aesar, Polyethylene Glycol 6000, PEG 6000) as an additive. The optimized polishing time was 9 min (see Fig. S1–1 and Tables S1–2†). The polished Cu-foil was then used as the substrate to synthesize graphene using the APCVD method. The substrate was first loaded into a tubular furnace and was vacuumed to $5 \times 10^{-3} \text{ Torr}$. The temperature was then ramped to $1060 \text{ }^\circ\text{C}$ at a rate of $30 \text{ }^\circ\text{C min}^{-1}$ under a mixed gas of H_2/Ar (20/80 sccm), and the pressure was kept at 540 mTorr. A surface annealing process was carried out to reduce and flatten the Cu surface under a mixed gas of H_2/Ar (30/1000 sccm) at 760 Torr for 30 min. During the graphene growth process, the gas atmosphere was switched to $\text{CH}_4/\text{H}_2/\text{Ar}$ (0.5/30/1000 sccm) at 760 Torr for 7 min. Then, it was cooled to room temperature under H_2/Ar (30/1000 sccm) flow to complete the process (see Fig. S1–2† for detailed steps of the process).

The transferring procedure for suspended graphene

The transferring process was based on the frequently used approach of spin coating (step 1: 500 rpm for 10 s; step 2: 1000 rpm for 60 s) a supporting layer of poly(methyl methacrylate) (PMMA-A4, MicroCHEM) on the as-grown graphene/Cu substrate, followed by a baking step at $80 \text{ }^\circ\text{C}$ for 5 min. The Cu substrate was etched away by 2 wt% ammonium persulfate

(J. T. Baker), followed by placing it in a large amount of DI water to dilute the residue. The graphene\PMMA film was transferred onto the target substrate (another Cu\graphene substrate), and then it was immediately dried using high speed spinning (step 1: 500 rpm for 10 s, and step 2: 1000 rpm for 60 s) to remove the water film between graphene\PMMA and the substrate followed by baking at 80 °C for 10 min. To release the internal strain, a reflow process was carried out by dropping PMMA on the surface and drying. The sample was immersed in warm acetone for 10 min to remove PMMA. Then, it was loaded into a furnace for thermal annealing under H₂/Ar (20/80 sccm) at 450 °C for 40 min. 5 layered graphene was realized by repeating the layer-by-layer stacking approach according to the aforementioned procedures. The Si nano-pillar substrates were prepared using electron beam lithography, followed by the reactive iron etching (RIE) process.

To obtain large area suspended graphene samples, Cu\5L-graphene\PMMA was subjected to an etching step to remove the Cu followed by DI water cleaning; then, it was transferred to a substrate with a hole (*e.g.*, a stainless steel plate 500 μm in thickness with an array of holes ranging from 20 μm to 1.5 mm in diameter) and dried at 80 °C for 10 min. The bubbling transfer process was another method we employed, where the graphene\PMMA layers were delaminated from the Cu substrate using an electrochemical method in 1 M NaOH solution, and the voltage bias was constant at 2.3 V.

The most important step was to remove the PMMA supporting layer. Here, the substrate was placed upside down across two glass slides (2 mm in thickness). Acetone was streamed at a gentle flow through the underlying channel and fully contacted the graphene\PMMA surface through controlling the flow rate at 1.7 mL s⁻¹ with a peristaltic pump for 10 min. Then, acetone was replaced by a low surface tension solvent, *i.e.*, C₄F₉OCH₃ (3 M, Novec 7100), to remove the acetone residue and was subsequently dried in the atmosphere. Finally, the sample was loaded into a furnace for an additional annealing step under H₂/Ar (20/80 sccm) at 450 °C under 540 mTorr for 40 min. The direct thermal decomposition method also followed the same annealing conditions.

The fabrication and characterization of a capacitive pressure sensor device

To fabricate the pressure sensor, the 5L-graphene membrane was transferred onto a quartz substrate with a 1.5 mm diameter hole. The substrate was then bonded onto a glass substrate, where the spacing between the quartz and the glass was adjusted to be 80 μm using a spacer tape. The edge of the sample was carefully sealed with silicone gel to prevent gas leakage from the edges. A gas inlet pipe (500 μm in diameter) and pressure gauge were integrated on the device, where a gas flow rate of 3.3 μL s⁻¹ was controlled. To measure the response of the pressure sensor, a Cu electrode was placed above the suspended graphene membrane at a distance of 160 μm. The capacitance was measured at a voltage ranging from -40 V to 40 V with a stimulated frequency of 20 Hz–2 MHz in an Agilent electrical meter (E4980A).

Material characterization

AFM was performed using a Bruker Innova system to characterize the thicknesses of the as-prepared multi-layered graphene films. Raman spectra were collected using a Horiba HR 550 confocal Raman microscope system (laser excitation wavelength = 532 nm; laser spot-size ~0.5 μm). The Raman scattering peak of Si at 520 cm⁻¹ was used as a reference for wavenumber calibration. The chemical configurations were determined using an X-ray photoelectron spectrometer (XPS, Phi V6000). The XPS measurements were performed using a Mg Kα X-ray source for sample excitation. The energies were calibrated relative to the C 1s peak to eliminate charging of the sample during analysis. SEM was carried out using a JEOL-6330F, and TEM observation was carried out using a JEOL-2010F with an accelerating voltage of 200 keV. Electrical conductivity, carrier concentration and mobility measurements were carried out on a Hall measurement system (Swin HALL8800). UV-vis-NIR transmittance spectra were obtained using a spectrophotometer (Jasco V670).

Acknowledgements

This research was supported by the Ministry of Science and Technology, Taiwan (102-2221-E-008-113-MY3). JL acknowledges support by NSF CBET-1240696 and DMR-1120901.

References

- 1 K. E. Mueggenburg, X.-M. Lin, R. H. Goldsmith and H. M. Jaeger, *Nat. Mater.*, 2007, **6**, 656–660.
- 2 J. He, P. Kanjanaboos, N. L. Frazer, A. Weis, X.-M. Lin and H. M. Jaeger, *Small*, 2010, **6**, 1449–1456.
- 3 K. C. Ng, I. B. Udagedara, I. D. Rukhlenko, Y. Chen, Y. Tang, M. Premaratne and W. Cheng, *ACS Nano*, 2012, **6**, 925–934.
- 4 Y. Chen, Z. Ouyang, M. Gu and W. Cheng, *Adv. Mater.*, 2013, **25**, 80–85.
- 5 W. Cheng, M. J. Campolongo, J. J. Cha, S. J. Tan, C. C. Umbach, D. A. Muller and D. Luo, *Nat. Mater.*, 2009, **8**, 519–525.
- 6 K. S. Novoselov, A. K. Geim, S. V. Morozov, D. Jiang, Y. Zhang, S. V. Dubonos, I. V. Grigorieva and A. A. Firsov, *Science*, 2004, **306**, 666–669.
- 7 K. I. Bolotin, K. J. Sikes, Z. Jiang, M. Klima, G. Fudenberg, J. Hone, P. Kim and H. L. Stormer, *Solid State Commun.*, 2008, **146**, 351–355.
- 8 C. Lee, X. Wei, J. W. Kysar and J. Hone, *Science*, 2008, **321**, 385–388.
- 9 A. A. Balandin, S. Ghosh, W. Bao, I. Calizo, D. Teweldebrhan, F. Miao and C. N. Lau, *Nano Lett.*, 2008, **8**, 902–907.
- 10 W. Bao, F. Miao, Z. Chen, H. Zhang, W. Jang, C. Dames and C. N. Lau, *Nat. Nanotechnol.*, 2009, **4**, 562–566.

- 11 K. V. Zakharchenko, M. I. Katsnelson and A. Fasolino, *Phys. Rev. Lett.*, 2009, 102.
- 12 J. C. Meyer, A. K. Geim, M. I. Katsnelson, K. S. Novoselov, T. J. Booth and S. Roth, *Nature*, 2007, **446**, 60–63.
- 13 C. N. Lau, W. Bao and J. Velasco Jr., *Mater. Today*, 2012, **15**, 238–245.
- 14 J. S. Bunch, A. M. van der Zande, S. S. Verbridge, I. W. Frank, D. M. Tanenbaum, J. M. Parpia, H. G. Craighead and P. L. McEuen, *Science*, 2007, **315**, 490–493.
- 15 P. Li, B. Zhang and T. Cui, *Biosens. Bioelectron.*, 2015, **72**, 168–174.
- 16 B. M. Venkatesan and R. Bashir, *Nat. Nanotechnol.*, 2011, **6**, 615–624.
- 17 A. D. Smith, F. Niklaus, A. Paussa, S. Vaziri, A. C. Fischer, M. Sterner, F. Forsberg, A. Delin, D. Esseni, P. Palestri, M. Ostling and M. C. Lemme, *Nano Lett.*, 2013, **13**, 3237–3242.
- 18 Y. D. Kim, H. Kim, Y. Cho, J. H. Ryoo, C.-H. Park, P. Kim, Y. S. Kim, S. Lee, Y. Li, S.-N. Park, Y. Shim Yoo, D. Yoon, V. E. Dorgan, E. Pop, T.F. Heinz, J. Hone, S.-H. Chun, H. Cheong, S. W. Lee, M.-H. Bae and Y. D. Park, *Nat. Nanotechnol.*, 2015, **10**, 676–681.
- 19 M. Freitag, T. Low and P. Avouris, *Nano Lett.*, 2013, **13**, 1644–1648.
- 20 J. S. Bunch, S. S. Verbridge, J. S. Alden, A. M. van der Zande, J. M. Parpia, H. G. Craighead and P. L. McEuen, *Nano Lett.*, 2008, **8**, 2458–2462.
- 21 K. Celebi, J. Buchheim, R. M. Wyss, A. Droudian, P. Gasser, I. Shorubalko, J.-I. Kye, C. Lee and H. G. Park, *Science*, 2014, **344**, 289–292.
- 22 J. M. Yuk, J. Park, P. Ercius, K. Kim, D. J. Hellebusch, M. F. Crommie, J. Y. Lee, A. Zettl and A. P. Alivisatos, *Science*, 2012, **336**, 61–64.
- 23 C. Wang, Q. Qiao, T. Shokuhfar and R. F. Klie, *Adv. Mater.*, 2014, **26**, 3410–3414.
- 24 J. Park, H. Park, P. Ercius, A. F. Pegoraro, C. Xu, J. W. Kim, S. H. Han and D. A. Weitz, *Nano Lett.*, 2015, **15**, 4737–4744.
- 25 S. Buckhout-White, J. T. Robinson, N. D. Bassim, E. R. Goldman, I. L. Medintz and M. G. Ancona, *Soft Matter*, 2013, **9**, 1414–1417.
- 26 K. Kim, Z. Lee, W. Regan, C. Kisielowski, M. F. Crommie and A. Zettl, *ACS Nano*, 2011, **5**, 2142–2146.
- 27 P. Y. Huang, C. S. Ruiz-Vargas, A. M. van der Zande, W. S. Whitney, M. P. Levendorf, J. W. Kevek, S. Garg, J. S. Alden, C. J. Hustedt, Y. Zhu, J. Park, P. L. McEuen and D. A. Muller, *Nature*, 2011, **469**, 389–392.
- 28 P. Li, B. Zhang and T. H. Cui, *Biosens. Bioelectron.*, 2015, **72**, 168–174.
- 29 C.-K. Lee, Y. Hwangbo, S.-M. Kim, S.-K. Lee, S.-M. Lee, S.-S. Kim, K.-S. Kim, H.-J. Lee, B.-I. Choi, C.-K. Song, J.-H. Ahn and J.-H. Kim, *ACS Nano*, 2014, **8**, 2336–2344.
- 30 Y. Zhang, R. Howver, B. Gogoi and N. Yazdi, A high-sensitive ultra-thin MEMS capacitive pressure sensor, in *Solid-State Sensors, Actuators and Microsystems Conference (TRANSDUCERS), 16th International, 5–9 June 2011*, 2011, pp. 112–115, DOI: 10.1109/TRANSDUCERS.2011.5969151.
- 31 A. Reserbat-Plantey, D. Kalita, Z. Han, L. Ferlazzo, S. Autier-Laurent, K. Komatsu, C. Li, R. Weil, A. Ralko, L. Marty, S. Guéron, N. Bendiab, H. Bouchiat and V. Bouchiat, *Nano Lett.*, 2014, **14**, 5044–5051.
- 32 L. Gao, W. Ren, H. Xu, L. Jin, Z. Wang, T. Ma, L.-P. Ma, Z. Zhang, Q. Fu, L.-M. Peng, X. Bao and H.-M. Cheng, *Nat. Commun.*, 2012, **3**, 699.
- 33 S. Saleh, A. Zaki, H. Elsemary and S. Ahmad, Modeling of Sensitivity of fabricated Capacitive Pressure Sensor, in *IECON 2006 – 32nd Annual Conference on IEEE Industrial Electronics*, 6–10 Nov. 2006, Paris, 2006, pp. 3166–3169, DOI: 10.1109/IECON.2006.347955.
- 34 Y. H. Wu and C. H. Chien, *Thesis for Master of Science*, Tatung University, 2008.
- 35 Q. Zhou, J. Zheng, S. Onishi, M. F. Crommie and A. K. Zettl, *Proc. Natl. Acad. Sci. U. S. A.*, 2015, **112**, 8942–8946.